IMPLEMENTATION AND TESTING OF THREE ENGINEERING MODELS OF TURBULENCE

Adam Jirásek*

This article deals with the implementation and testing of three eddy-viscosity models of turbulence. One model is a model using Boussinesq hypothesis, two other models are EARSM and EARSM with curvature corrections. Outlined is a brief description of the theory behind both Boussinesq hypothesis and EARSM models of turbulence. The models and their implementation were then evaluated in the case of flow around the RAE 2822 airfoil and around the M6 wing, comparing computational data to each other and to the experimental data.

Key words: *turbulence, Boussinesq hypothesis, EARSM, EARSM with curvature corrections*

1. Introduction

The turbulence models are an important part of the Computational Fluid Dynamics, CFD, used to model the turbulent flow. This can be used during early stage of the design prior to manufacturing of the model and wind tunnel test. This stage can be and usually is extended and run simultaneously with the experimental testing. The next task is a post-design analysis of the unexpected behavior observed during wind tunnel or flight test. Especially demanded is the analysis of the off-design conditions [1]. Every task has its own specifics and requires in some ways different approaches and need an analyst with relevant skills to carry out the computations and being confident enough to interpret the results.

The CFD user is at the beginning facing a large number of uncertainties and is questioning basic processes such as a mesh generation, if given, the choice of the numerical scheme and

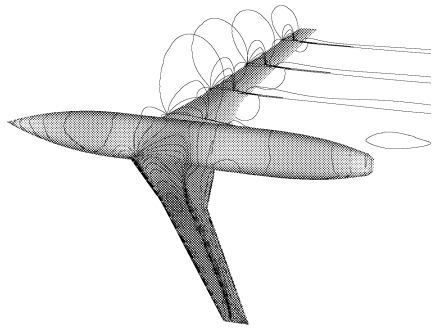

Fig.1: Example of a conceptual design calculations, wing-body configuration

* A. Jirásek, Research Engineer, Defence and Security, Systems Technolgy, Swedish Defence Research Agency FOI, Stockholm, SE-164 90, Sweden

very often the choice of the model of turbulence. Even after spending longer time in CFD one is usually asking a question which model of turbulence is the best or which model should be used in some particular problem. This question, however does not have a unique answer and uncertainty always remains. There is simply no universal model suited for all types of flows. Rather then trying to answer this question it is better to try to understand the way how the turbulence models are derived, be aware of their possible limitations and in the light of this knowledge make an appropriate interpretation of a result.

This article describes three different eddy-viscosity engineering turbulence models – one based on Boussinesq hypothesis, one Explicit Algebraic Reynolds Stress Model, EARSM, and one EARSM corrected for high curvature flows. These models represent two typical approaches in modeling of the turbulent flow with two-equations models of turbulence. The models were implemented and used in 2D and 3D flow. Their results were compared to each other and to the experimental data.

2. Turbulence modeling

This paragraph gives a brief description of a turbulence modeling of two-equation models. For detailed description the reader is referred to [2]. Concerning two-equation models of turbulence there are two main streams. The first is a direction leading to the eddy-viscosity models based on Boussinesq hypothesis. The second direction goes towards more complicated models called Algebraic Reynolds stress models or more specifically Explicit Algebraic Reynolds stress models.

The development of turbulence models can start at the transport equation for Reynolds stress

$$\frac{\mathrm{d}\,\overline{u_i\,u_j}}{\mathrm{d}t} = \mathcal{P}_{ij} - \epsilon_{ij} + \Pi_{ij} + \mathcal{D}_{ij}\ . \tag{1}$$

Defining the variable turbulent energy $k = \overline{u_i\,u_i}/2$ and taking the half of the trace of system (1) the equation for Reynolds stress is reduced to the equation for the turbulent energy k

$$\frac{\mathrm{d}k}{\mathrm{d}t} = \mathcal{P}_{\mathrm{k}} - \epsilon + \mathcal{D}_{\mathrm{k}}\ . \tag{2}$$

It includes the production of turbulent energy $\mathcal{P}_{\mathrm{k}}$, the dissipation rate ϵ and the diffusion $\mathcal{D}_k$ and is the equation for turbulent energy k used in one and more equations turbulence models. To solve the problem of the modeling of the Reynolds stresses $\overline{u_i\,u_j}$, Boussinesq [3] formulated hypothesis which is today referred to as the Boussinesq hypothesis. This approximation assumes that the axis of Reynolds-stress tensor τ_i are coincident with those of strain-rate tensor S_{ij}. He then formulated well known relation between the Reynolds stress tensor and the strain-rate tensor which is analogous to the relation valid in laminar flow

$$\tau_{ij} = -\overline{u_i\,u_j} = 2\,\nu_{\mathrm{T}}\,S_{ij} - \frac{2}{3}\,k\,\delta_{ij} \tag{3}$$

where ν_{T} is called the kinematic eddy viscosity. The ν_{T} is in one and more equations models of turbulence a function of the turbulent energy k and other additional parameters. The turbulence models which use the equation (3) are then called the eddy viscosity models based on Boussinesq hypothesis. For overview of these models see for example [2, 4].

The assumption of the linear relation between strain-rate and Reynolds stress (3) gives good results in the flow where the Knudsen number is $Kn = l_{\mathrm{mfp}}/L \ll 1$. The l_{mfp} is the

mean free path and L is the characteristic length scale of the mean flow. In certain types of flows this assumption is, however, no more valid. It is in the flows with sudden changes in mean strain-rate, flow over curved surfaces, flow in duct with secondary motion, flow in rotating fluid, three-dimensional flows and flows with boundary layer separation.

More accurate description of the Reynolds stress tensor can be obtained using the stress-transport models which are referred to as a second-order closure or second-moment closure models. They are usually derived from the equation (1). It can be also transformed to the equation for anisotropy a_{ij}.

$$a_{ij} \equiv \frac{\overline{u_i\, u_j}}{k} - \frac{2}{3}\,\delta_{ij}\ . \tag{4}$$

Including terms for the pressure strain-tensor Π_{ij} and the dissipation rate ϵ_{ij} the equation (1) can have form

$$k\left(\frac{\mathrm{d}a_{ij}}{\mathrm{d}t} - \mathcal{D}_{ij}^{(a)}\right) = \left(\mathcal{P}_{ij} - \frac{\overline{u_i\, u_j}}{k}\,\mathcal{P}\right) - \left(\epsilon_{ij} - \frac{\overline{u_i\, u_j}}{k}\,\epsilon\right) + \Pi_{ij}\ . \tag{5}$$

This is a system of the differential equations for anisotropy a_{ij} and the turbulence models which are based on this equation are called the Differential Reynolds Stress Models (DRSM). The modeling of Reynolds stress tensor is not needed because its value is obtained directly from the solution. What arises is a need of the modeling of additional terms such as pressure strain-tensor Π_{ij} and the dissipation rate ϵ_{ij} Using quasi-linear models for Π_{ij} and dissipation rate anisotropy $e_{ij} = \epsilon_{ij}/\epsilon - 2/3\,\delta_{ij}$ the equation (5) can be reformulated to

$$\begin{aligned}\tau\left(\frac{\mathrm{d}a_{ij}}{\mathrm{d}t} - \mathcal{D}_{ij}^{(a)}\right) = A_0\Bigg[\left(A_3 + A_4\,\frac{\mathcal{P}}{\epsilon}\right)a_{ij} + A_1\,\widetilde{S}_{ij} - \left(a_{ik}\,\widetilde{\Omega}_{kj} - \widetilde{\Omega}_{ik}\,a_{kj}\right) + \\ + A_2\left(a_{ik}\,\widetilde{S}_{kj} - \widetilde{S}_{ik}\,a_{kj} - \frac{2}{3}\,a_{kl}\,\widetilde{S}_{lk}\,\delta_{ij}\right)\Bigg]\end{aligned} \tag{6}$$

which is an equation of Reynolds stress models* and model constants $A_{(0-4)}$. With the assumption that the anisotropy in flow-field varies slowly the left hand side of equation (6) can be neglected and the equation (6) takes the form

$$\begin{aligned}0 = A_0\Bigg[\left(A_3 + A_4\,\frac{\mathcal{P}}{\epsilon}\right)a_{ij} + A_1\,\widetilde{S}_{ij} - \left(a_{ik}\,\widetilde{\Omega}_{kj} - \widetilde{\Omega}_{ik}\,a_{kj}\right) + \\ + A_2\left(a_{ik}\,\widetilde{S}_{kj} - \widetilde{S}_{ik}\,a_{kj} - \frac{2}{3}\,a_{kl}\,\widetilde{S}_{lk}\,\delta_{ij}\right)\Bigg]\ .\end{aligned} \tag{7}$$

The models which are using this equation are called the Algebraic Reynolds Stress Models, ARSM. The equation (7) is then reformulated as an explicit one using a suitable model for anisotropy. It can have a form

$$\begin{aligned}\boldsymbol{a} = \beta_1\,\widetilde{\mathbf{S}} + \beta_2\left(\widetilde{\mathbf{S}}^2 - \frac{1}{3}\,\Pi_{\widetilde{\mathbf{S}}}\,\mathbf{I}\right) + \beta_3\left(\widetilde{\mathbf{\Omega}}^2 - \frac{1}{3}\,\Pi_{\widetilde{\Omega}}\,\mathbf{I}\right) + \beta_4\left(\widetilde{\mathbf{S}}\,\widetilde{\mathbf{\Omega}} - \widetilde{\mathbf{\Omega}}\,\widetilde{\mathbf{S}}\right) + \\ + \beta_5\left(\widetilde{\mathbf{S}}^2\,\widetilde{\mathbf{\Omega}} + \widetilde{\mathbf{\Omega}}\,\widetilde{\mathbf{S}}^2\right) + \beta_6\left(\widetilde{\mathbf{S}}\,\widetilde{\mathbf{\Omega}}^2 + \widetilde{\mathbf{\Omega}}^2\,\widetilde{\mathbf{S}} - \frac{2}{3}\,IV\,\mathbf{I}\right) + \\ + \beta_7\left(\widetilde{\mathbf{S}}^2\,\widetilde{\mathbf{\Omega}}^2 + \widetilde{\mathbf{\Omega}}^2\,\widetilde{\mathbf{S}}^2 - \frac{2}{3}\,V\,\mathbf{I}\right) + \beta_8\left(\widetilde{\mathbf{S}}\,\widetilde{\mathbf{\Omega}}\,\widetilde{\mathbf{S}}^2 + \widetilde{\mathbf{S}}^2\,\widetilde{\mathbf{\Omega}}\,\widetilde{\mathbf{S}}\right) + \\ + \beta_9\left(\widetilde{\mathbf{\Omega}}\,\widetilde{\mathbf{S}}\,\widetilde{\mathbf{\Omega}}^2 + \widetilde{\mathbf{\Omega}}^2\,\widetilde{\mathbf{S}}\,\widetilde{\mathbf{\Omega}}\right) + \beta_{10}\left(\widetilde{\mathbf{\Omega}}\,\widetilde{\mathbf{S}}^2\,\widetilde{\mathbf{\Omega}}^2 + \widetilde{\mathbf{\Omega}}^2\,\widetilde{\mathbf{S}}^2\,\widetilde{\mathbf{\Omega}}\right)\end{aligned} \tag{8}$$

* The Reynolds Stress Models can be defined in terms of the strain-rate tensor $\mathbf{S}$ also.

and is a basis for the Explicit Algebraic Reynolds Stress Models, EARSM. The Reynolds stress $\overline{u_i\,u_j}$ is then a function of the anisotropy a_{ij}. For more details see for example Wilcox [2].

There is another important difference in behavior of the models based on Boussinesq hypothesis and the EARSM models. The production of turbulent energy in Boussinesq hypothesis based models is a function of $P_\mathrm{k} \approx \mathbf{S}^2$ meanwhile in the EARSM the dependency is $P_\mathrm{k} \approx \mathbf{S}$. The models with $P_\mathrm{k} \approx \mathbf{S}^2$ therefore use limiters for production P_k which is active mainly in the vicinity of shock wave. These limiters, however, must be used with care. Kozel et al. [5] showed the strong dependency of turbulent energy on the choice of limiter giving rise to rather large differences in solution. The EARSM does not need any limiter.

2.1. Kok TNT k–ω model of turbulence

The TNT k–ω was developed by Kok [6]. It is based on the classical k–ω model [2] with two equations for the turbulent energy k and the specific dissipation rate ω

$$\frac{\partial \rho\, k}{\partial t} + \frac{\partial \rho\, k\, u_i}{\partial x_i} = \frac{\partial}{\partial x_i}\left[(\mu + \sigma_\mathrm{k}\,\mu_\mathrm{T})\,\frac{\partial k}{\partial x_i}\right] - \beta^*\,\rho\,\omega\,k + \mathcal{P}_\mathrm{k}\ , \tag{9}$$

$$\frac{\partial \rho\,\omega}{\partial t} + \frac{\partial \rho\,\omega\, u_i}{\partial x_i} = \frac{\partial}{\partial x_i}\left[(\mu + \sigma_\omega\,\mu_\mathrm{T})\,\frac{\partial \omega}{\partial x_i}\right) - \beta\,\rho\,\omega^2 + \mathcal{P}_\omega + C_\mathrm{D}\ . \tag{10}$$

The TNT variant contains the term C_D called the cross-diffusion term which makes the model to a certain extent insensitive to free stream levels of turbulence. The Reynolds stress is then calculated

$$\rho\,\tau_{ij} = 2\,\mu_\mathrm{T} S_{ij} - \frac{2}{3}\,\rho\,k\,\delta_{ij} \tag{11}$$

with dynamic eddy viscosity $\mu_\mathrm{T} = \rho\,k/\omega$. For more details on the model including definition of terms P_k and P_ω and model constants see [6].

2.2. EARSM model

The EARSM model of turbulence proposed in [7] formulates an expression for the Reynolds stress tensor in terms of the strain-rate $\mathbf{S}$ and the extra anisotropy tensor $\mathbf{a}^{(\mathrm{ex})}$

$$\rho\,\tau_{ij} = \rho\,k\left(2\,C_\mu^{\mathrm{eff}}\,\widetilde{S}_{ij} - \frac{2}{3}\,\delta_{ij} - a_{ij}^{(\mathrm{ex})}\right) = 2\,\mu_\mathrm{T}^{\mathrm{eff}}\,S_{ij} - \frac{2}{3}\,\rho\,k\,\delta_{ij} - \rho\,k\,a_{ij}^{(\mathrm{ex})}\ . \tag{12}$$

The multiplier C_μ^{eff} in equation (12) is a function strain-rate tensor $\mathbf{S}$ and rotation $\mathbf{\Omega}$

$$C_\mu^{\mathrm{eff}} = -\frac{1}{2}\,(\beta_1 + \Pi_\Omega\,\beta_6)\ . \tag{13}$$

The definition of extra anisotropy $\mathbf{a}^{(\mathrm{ex})}$ is taken from equation (8)

$$\begin{aligned}\boldsymbol{a}^{(\mathrm{ex})} = {}& \beta_3\left(\widetilde{\mathbf{\Omega}}^2 - \frac{1}{3}\,\Pi_{\widetilde{\Omega}}\,\mathbf{I}\right) + \beta_4\left(\widetilde{\mathbf{S}}\,\widetilde{\mathbf{\Omega}} - \widetilde{\mathbf{\Omega}}\,\widetilde{\mathbf{S}}\right) + \\ & + \beta_6\left(\widetilde{\mathbf{S}}\,\widetilde{\mathbf{\Omega}}^2 + \widetilde{\mathbf{\Omega}}^2\,\widetilde{\mathbf{S}} - \Pi_{\widetilde{\Omega}}\,\widetilde{\mathbf{S}} - \frac{2}{3}\,IV\,\mathbf{I}\right) + \beta_9\left(\widetilde{\mathbf{\Omega}}\,\widetilde{\mathbf{S}}\,\widetilde{\mathbf{\Omega}}^2 - \widetilde{\mathbf{\Omega}}^2\,\widetilde{\mathbf{S}}\,\widetilde{\mathbf{\Omega}}\right)\end{aligned} \tag{14}$$

where the $\widetilde{\mathbf{S}}$ and $\widetilde{\mathbf{\Omega}}$ are normalized strain-rate and rotational tensors defined as $\widetilde{\mathbf{S}} = \tau\,\mathbf{S}$ and $\widetilde{\mathbf{\Omega}} = \tau\,\mathbf{\Omega}$. The turbulent time scale is defined

$$\tau = \max\left(\frac{k}{\epsilon}, C_\tau\sqrt{\frac{\mu}{\rho\,\epsilon}}\right)\ . \tag{15}$$

The definition of invariants $\Pi_{\widetilde{\mathrm{S}}}$, $\Pi_{\widetilde{\Omega}}$ and IV and coefficients β_{1-9} as well as model constants used in the EARSM is given in [7]. The model in this implementation is combined with standard $k-\omega$ turbulence model [2]. Another interesting EARSM implementation with very good features in separated flow was recently published in [8].

2.3. Curvature Corrections of the EARSM model

The assumption of a weak equilibrium which simplifies the equation (6) to equation (7) becomes inaccurate in the flow-field with high curvature. This assumption can be additionally imposed in a general curvilinear system. The advection of the anisotropy is defined in a curvilinear system as

$$\frac{\mathrm{d}\mathbf{a}}{\mathrm{d}t} = \mathbf{T}^t\,\frac{\mathrm{d}\mathbf{T}\,\mathbf{a}\,\mathbf{T}^{\mathrm{T}}}{\mathrm{d}t}\,\mathbf{T} - \left(\mathbf{a}\,\mathbf{\Omega}^{(\mathrm{r})} - \mathbf{\Omega}^{(\mathrm{r})}\,\mathbf{a}\right) \tag{16}$$

where $\mathbf{T}$ is a transformation matrix of the orthogonal system $(\mathbf{t}, \mathbf{n}, \mathbf{s})$ to curvilinear system $(\hat{\mathbf{t}}, \hat{\mathbf{n}}, \hat{\mathbf{s}})$ and

$$\mathbf{\Omega}^{(\mathrm{r})} = \frac{\mathrm{d}\mathbf{T}^{\mathrm{T}}}{\mathrm{d}t}\,\mathbf{T}\ . \tag{17}$$

The correction is then implemented into the EARSM models by replacing the term $\mathbf{\Omega}^*$ in Eq. (6) for the term $\mathbf{\Omega}$ where

$$\mathbf{\Omega}^* = \mathbf{\Omega} - \frac{\tau}{A_0}\,\mathbf{\Omega}^{(\mathrm{r})} \tag{18}$$

with A_0 being a model constant. Several models extending the EARSM models to flows with high curvature have been developed, see for example [9, 10, 11, 12]. The model used in this work was developed in [13] and is a strain-rate based coordinate system. Since the anisotropy tensor is a function of strain-rate tensor and tensor of rotation the equation (16) can be expressed in terms of the $\mathbf{S}$ and $\mathbf{S}\,\mathbf{\Omega}$

$$\frac{\mathrm{d}\mathbf{S}}{\mathrm{d}t} = \mathbf{T}^{\mathrm{T}}\,\frac{\mathrm{d}\mathbf{T}\,\mathbf{S}\,\mathbf{T}^{\mathrm{T}}}{\mathrm{d}t}\,\mathbf{T} - \left(\mathbf{S}\,\mathbf{\Omega}^{(\mathrm{r})} - \mathbf{\Omega}^{(\mathrm{r})}\,\mathbf{S}\right)\ . \tag{19}$$

The curvature correction $\mathbf{\Omega}^{(\mathrm{r})}$ is then found as a solution of the equation (19) in sense of minimizing the variations of $\mathbf{S}$.

3. Flow solver

The flow solver is structured multiblock solver for Euler and Navier-Stokes equation based on upwind flux vector splitting scheme of van Leer [14, 15] with third order accurate MUSCL interpolation of the variables on the cell faces. The time integration is based on Runge-Kutta scheme of Jameson, Schmidt and Turkel [16, 17]. It is equipped with a local low-speed preconditioner based on entropy, implicit residual smoothing, multigrid with bilinear restriction and prolongation operators, full multigrid and dual-time-stepping [18, 17, 19, 20, 21]. All calculations were performed using the W multigrid at three-level grids or double W cycle at

four-level grids. The values of *CFL* number varied from $CFL = 2$ to $CFL = 3.5$ depending mainly on the turbulence model. One million grid case with $k-\omega$ TNT model (M6 test case) took on the ordinary PC computer with Pentium processor at frequency 2 GHz about 14 hours to a fully converged solution. EARSM model added between 30 % and 40 % in the computational time depending on the computational case and curvature corrections almost doubled the amount of the computational time compared to the $k-\omega$ TNT model.

The boundary conditions used for the external aerodynamics cases are non-slip boundary condition on the wall and the characteristics boundary conditions at a far-field boundary. The transition to turbulence was prescribed by putting the value of the production of turbulent energy $P_\mathrm{k} = 0$.

4. Test cases

The flow solver was tested in the case of two airfoils and the M6 wing.

4.1. Case1: RAE 2822 airfoil

The first test case is the flow around the RAE 2822 airfoil at angle of attack $\alpha_\infty = 2.79°$, Mach number $M_\infty = 0.73$ and Reynolds number $Re = 6.5{\times}10^6$ with transition of the boundary layer at 3 % of chord [22]. The mesh around the airfoil is a hyperbolic mesh with high orthogonality on the surface of the airfoil [23]. Figure 2 shows a closer view on the grid. Hyperbolic grid generation enables also direct control of the cell size and mesh cell growth in a wall normal direction which is important especially in the boundary layer. Moitra [24]

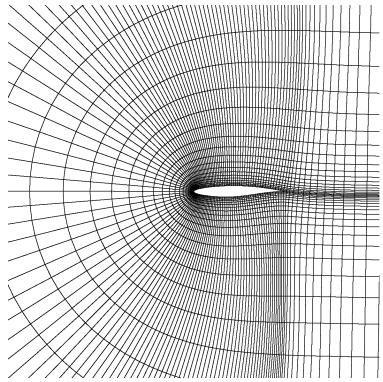

Fig.2: Detail of computational mesh, the RAE 2822 airfoil

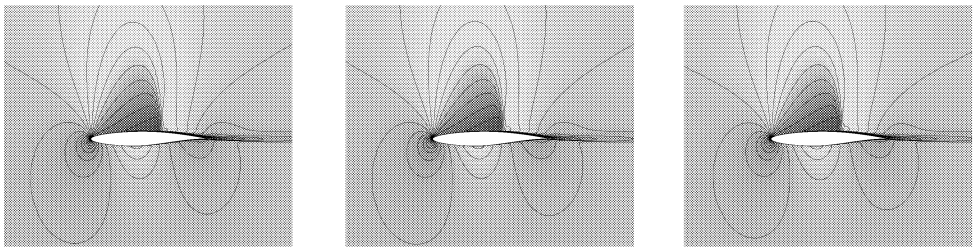

(a) **TNT** (b) **EARSM** (c) **EARSM + CC**

Fig.3: Isolines of Mach number, the RAE 2822 airfoil

defined the rules for the mesh generation for the flow around 2D high lift systems. The mesh around RAE 2822 airfoil follows his recommendation in most of areas but the trailing edge. The mesh around trailing edge is rather coarse which certainly affects the solution as discussed later. The isolines of Mach number for all three models are shown in figure 3. The similarity of the solutions is apparent. The difference takes place in the area of shock wave boundary layer interaction where both EARSM models predict small area of the flow separation – see friction coefficient in figure 4(b). The EARSM models predict also the different development of the friction coefficient in the flow-field downstream of the shock wave. All models predicts sudden increase of the friction at the very end of profile which is a consequence of poor grid resolution around trailing edge. The geometry with sharp trailing edge plays also an important role [25]. Figure 5 shows comparison of the velocity profiles in three positions. It shows the discrepance between the computational and experimental data increases in the regions of adverse pressure gradient. The EARSM models show better effect of adverse pressure gradient compared to the TNT $k-\omega$ model, however it is still insufficient.

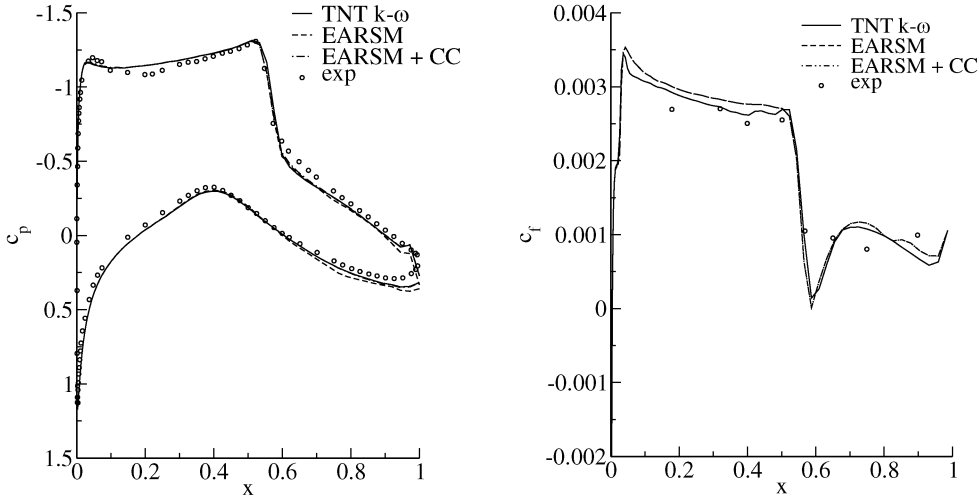

(a) **pressure coefficient** (b) **friction coefficient**

Fig.4: Pressure and friction coefficient, the RAE 2822 airfoil

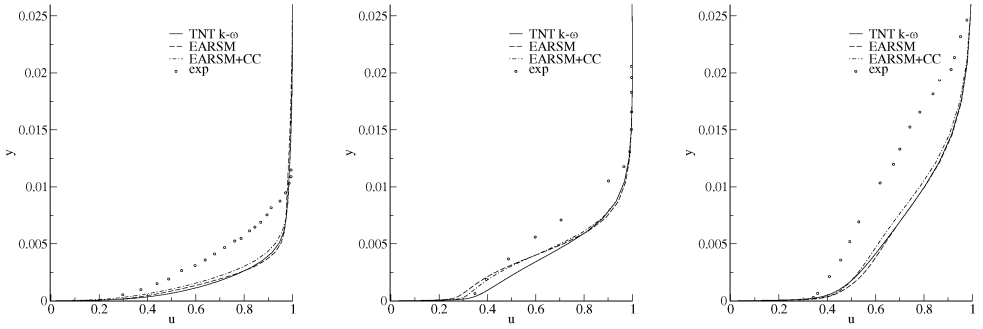

(a) 57.4%*c* (b) 65%*c* (c) 90%*c*

Fig.5: Velocity profiles in three positions of the chord, the RAE 2822 airfoil

4.2. Case2: AS2809 airfoil

The second case is the flow over the AS2809 profile tested at the Aeronautical Research and Test Institute, VZLÚ. The airfoil was calculated using the Kok TNT model at Mach number $M = 0.771$, angle of attack $\alpha_\infty = 3.12°$ and Reynolds number $Re = 2.18{\times}10^6$. The isolines of Mach number are shown in figure 6. The problem with prediction of the intensity of shock wave is very possibly caused by the low value of Reynolds number which have a strong effect on the shock-wave boundary layer interaction. The airfoil was calculated with fixed transition and does not take to account the length of the transitional area which at these values of Reynolds number certainly plays an important role. It can be expected that using some model for transition would improve the result. Nevertheless the prediction of pressure distribution on the airfoil is still fairly good.

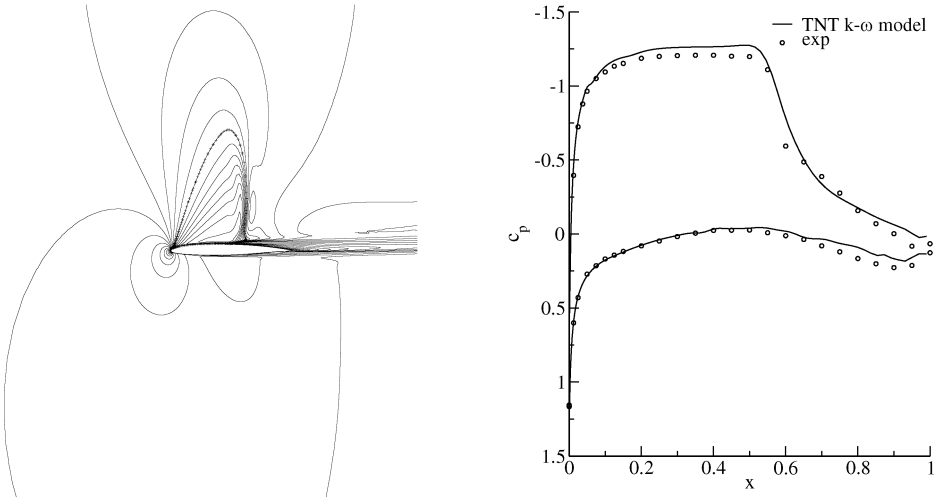

(a) **isolines of Mach number** (b) **pressure coefficient**

Fig.6: AS2809 airfoil, $M = 0.771$, $\alpha_\infty = 3.12°$, $Re = 2.18{\times}10^6$

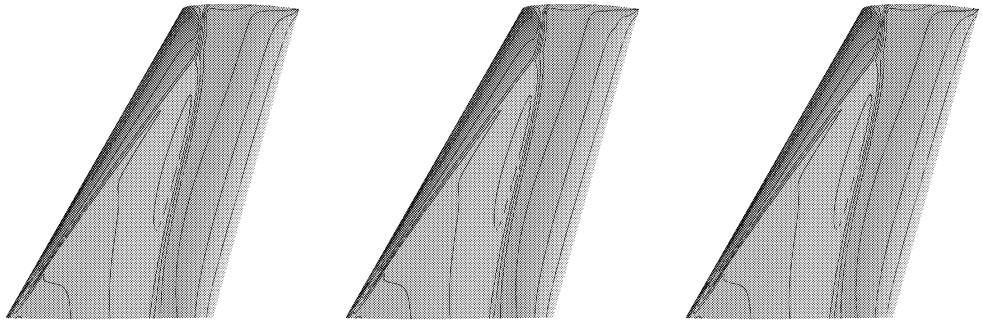

(a) **TNT** (b) **EARSM** (c) **EARSM + CC**

Fig.7 Isolines of pressure coefficient on the surface, the M6 wing

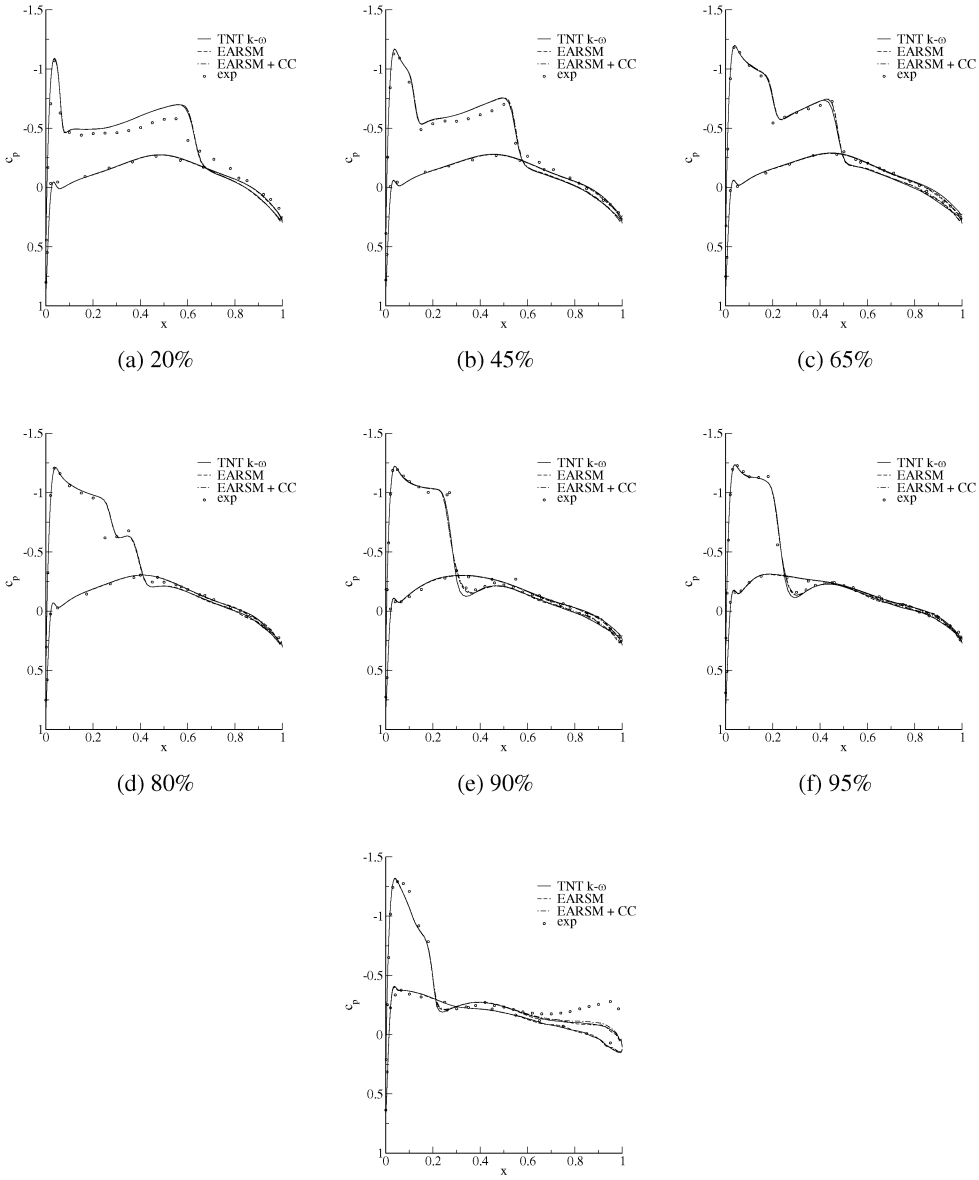

(a) 20% (b) 45% (c) 65%

(d) 80% (e) 90% (f) 95%

(e) 99%

Fig.8 Pressure coefficient compared to the experimental data, the M6 wing

4.3. Case3: M6 wing

The third case is a flow around the M6 wing at Mach number $M_\infty = 0.83$ and angle of attack $\alpha_\infty = 3.04°$. The Reynolds number is $Re = 11.6{\times}10^6$. The isolines of pressure coefficient on the wing surface show very similar patterns for all three models of turbulence. As in previous case there is not much variability between different turbulence models. The c_p coefficient in the cuts in different spanwise positions of the wing show good agreement with the experimental data. The differences between different turbulence models are marginal. The EARSM predicts better the flow expansion behind the shock wave especially in the

positions around end of the wing. This might be caused by better behavior of the EARSM models in vicinity of the shock waves. The disagreement with experimental data is visible in the cut in 99 % of the span. Although some differences between different models of turbulence are visible they are marginal compared to the gap between computational results and experimental data. Figure 9 shows streamlines restricted on the wing surface around the wing ending arc. The EARSM without curvature corrections tend to predict flow separation on the ending arc closer to the upper side of the wing. The pattern of TNT model is similar to the EARSM with curvature corrections.

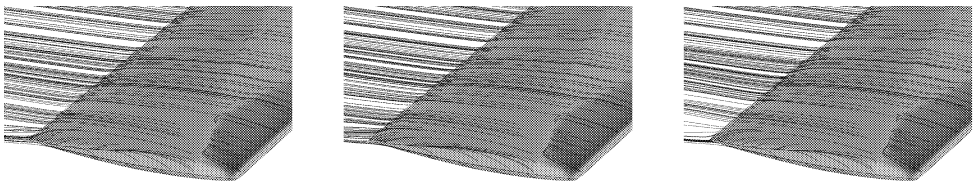

(a) **TNT** (b) **EARSM** (c) **EARSM + CC**

Fig.9: Streamlines of the flow around ending arc of the M6 wing

5. Conclusion

This article compare three different eddy viscosity models of turbulence, the $k-\omega$ TNT based on Boussinesq hypothesis, the $k-\omega$ EARSM model and its extension to high curvature flows. The three turbulence models were used to calculate the flow around two airfoils and flow around the M6 wing and the computational results were compared to experimental data. The three different turbulence models give very similar results. The EARSM model showed certain improvement over the $k-\omega$ TNT model especially in regions containing shock wave. It is due to better modeling of the production of turbulent energy in the vicinity of shocks. The consequence is also a better stability of EARSM model. Unfortunate is an additional computational expense. Curvature corrections did not introduce any substantial difference in the solutions. It is because the test cases where the EARSM with curvature corrections was tested have rather small areas of highly curved flows. However, in cases of highly curved flow such as a flow over delta wings, the curvature corrections may have a substantial effect. Curvature corrections added the substantial computational expense and unfortunately contribute to certain un-stability of the flow solver. The agreement with the experimental data for airfoils and the M6 wing was very good. In more difficult cases the choice of the model can, however, be a decisive factor determining the quality of the results.

References

[1] Spalart P.R.,Bogue D.R.: The role of CFD in aerodynamics, off-desing, The Aerounautical Journal, 2003

[2] Wilcox D.: Turbulence modeling in CFD, DCW Industries, La Canada, 2nd ed., 1999

[3] Boussinesq J.: Essai sur la theorie des eaux courantes, Mém. pres. acad. sci., 3rd eddition, Paris, XXIII, 46 1877

[4] Louda P.: Numerical Solution of Two-Dimensional and Three-Dimensional Turbulent Impinging Jet, Doctoral thesis, Faculty of Mechanical Engineering, Czech Technical University, Prague, 2002

[5] Kozel K., Louda P., Příhoda J.: Numerical modeling of turbulent flow through a turbine cascade, In: Proceeding of conference Engineering Mechanics, ed. I. Zoltarev, Svratka, CD-ROM 9 p., Czech Republic, 2004

[6] Kok J.: Resolving the Dependence on Freestream Values for the $k-\omega$ Turbulence model, AIAA Journal, Vol. 38, No. 7, July 2000
[7] Wallin S., Johansson A.V.: A Complete Explicit Algebraic Reynolds Stress Model for Incompressible and Compressible Turbulent Flows, Journal of Fluid Mechanics, Vol. 403, 2000, pp. 89–132
[8] Hellsten, A.: New Advanced $k-\omega$ Turbulence Model for High Lift Aerodynamics, AIAA Journal , Vol. 43, No. 9, 2005
[9] Girimaji S.S.: A Galilean invariant explicit algebraic Reynolds stress models for turbulent curved flows, Physics of Fluids, Vol. 9, No. 9, pp. 1067–1077, 1997
[10] Gatski T.B., Jongen T.: Nonlinear eddy viscosity and algebraic Reynolds stress models for solving complex turbulent flows, Progress in Aerospace Sciences, Vol. 36, No. 8, pp. 655–682, 2000
[11] Spalart P.R., Shur M.: On the sensation of turbulence models to rotation and curvature, Aerospace Science and Technology 1(5), pp. 297–302, 1997
[12] Hellsten A., Wallin S., Laine S.: Scrutinizing Curvature Corrections for Algebraic Reynolds Stress Models, AIAA Paper 2002-2963, 2002
[13] Wallin S., Johansson A.V.: Modelling streamline curvature effects in explixit algebraic Reynolds stress turbulence model, Heat and Fluid Flow, Vol. 23, pp. 712–730, 2002
[14] van Leer B.: Flux vector splitting for Euler equations, Eight international conference on numerical methods in fluid dynamics Achen: proceeding of conference, Rheinish-Westfischen Technische Hochschule, Achen, Germany, 1982
[15] Anderson W.K., Thomas J.L., van Leer B.: Comparison of finite volume flux vector splittings for the Euler equations, AIAA Journal, Vol. 24, No. 9, 1986
[16] Jameson A., Schmidt W., Turkel E.: Numerical Solution of Euler Equations by Finite Volume Methods Using Runge-Kutta Time Stepping Schemes, AIAA Paper 81-1259, 1981
[17] Swanson R.C., Turkel E.: Multistage Schemes with Multigrid for Euler and Navier-Stokes Equations, NASA TP 3631, 1997
[18] Turkel E., Vatsa V.N., Radespiel R.: Preconditioning Methods for Low-Speed Flow, NASA CR-201605, 1996
[19] Jirásek A.: The calculation of flow with low Mach numbers regions, Letecký zpravodaj, VZLÚ, 2001
[20] Jameson A.: Time dependent calculation using multigrid, with application to unsteady flows past airfoils and wing, AIAA Paper 91-1596, 1991
[21] Jirásek A.: Calculation of the inviscid unsteady flow around oscillating airfoil using implicit scheme, Letecký zpravodaj, VZLÚ, 2001
[22] Cook P.H., McDonald M.A., Firmin M.C.P.: Aerofoil 2822 – Presusre Distributions, Boundary Layer and Wake Measurements, AGARD Advisory Report, AR 138, 1979
[23] Jirásek A., Kladrubský M.: Generation of Grids for Calculation of Flow, Letecký zpravodaj, VZLÚ, 2000
[24] Moitra A.: Automated CFD Analysis of Two-Dimensional High-Lift Flow, Journal of Aircraft, Vol. 39, No. 4, July-August 2002
[25] Jirásek A., Eliasson P., Wallin S.: Computational Study of the High-Lift A-Airfoil, Journal of Aircraft, Vol. 38, No. 4, July-August 2001

Received in editor's office: January 6, 2006
Approved for publishing: July 11, 2006